ORIGINAL ARTICLE

Optimization of the controllable crystal size of iron/zeolite nanocomposites using a Box–Behnken design and their catalytic activity

Nurazni Amat Bahari[1] · Wan Nor Roslam Wan Isahak[1,2] · Mohd Shahbudin Masdar[1,2] · Muneer M. Ba-Abbad[3]

Abstract

Experimental conditions for the synthesis of an iron nanoparticle (NPs)–zeolite composite (hereinafter denoted as Fe/zeolite NPs) via sol–gel method were optimized using a Box–Behnken design to produce a high formic acid yield. The effects of various parameters, including weight ratio of starting materials (Fe and zeolite), volume of polyethylene glycol (PEG) as a surfactant, and calcination temperature, on controllable crystallite size, and the relationship between crystallite size and formic acid yield were studied. The crystal size, as the main parameter indicating formic acid yield, of Fe NPs was evaluated through polynomial regression. Results revealed that the optimum conditions for producing small Fe NPs based on the model were obtained at a weight ratio of Fe to zeolite of 62.5%, a PEG volume of 2 mL, and a calcination temperature of 500 °C. The experimental results (52.02 nm) versus the predicted results (58.30 nm) of the crystal size of Fe NPs under the optimum synthesis conditions were similar. Furthermore, 62.5% Fe/zeolite NPs with a crystal size of 52.02 nm produced the highest formic acid concentration from CO_2 hydrogenation. Conversely, 100% Fe/zeolite NPs had a smaller crystal size but exhibited a remarkably lower reaction performance. This high ratio of Fe and zeolite contributed to the increased agglomeration of Fe particles. The zeolite surface became fully covered and subsequently reduced the reactant interaction on catalyst surfaces. Highlights:

- Fe–zeolite nanocomposite was optimized using a Box–Behnken design.
- The polynomial regression model showed the optimum nanoparticle (NP) crystal size of 52.02 nm.
- Synthesis parameters significantly affected catalyst morphology and crystal.
- The effect of calcination plays an important role on crystal and particle size.
- The influence of NP crystallite size was evaluated in terms of formic acid production.

✉ Wan Nor Roslam Wan Isahak
 wannorroslam@ukm.edu.my

1 Research Centre for Sustainable Process Technology (CESPRO), Faculty of Engineering and Built Environment, Universiti Kebangsaan Malaysia, 43600 Bangi, Selangor, Malaysia

2 Chemical Engineering Programme, Faculty of Engineering and Built Environment, Universiti Kebangsaan Malaysia, 43600 Bangi, Selangor, Malaysia

3 Department of Chemical Engineering, Faculty of Engineering and Petroleum, Hadhramout University, Mukalla, Hadhramout, Yemen

Introduction

Iron oxide nanoparticles (NPs) include hematite (α-Fe_2O_3), maghemite (γ-Fe_2O_3), and magnetite (Fe_3O_4). Among them, α-Fe_2O_3 is the most useful and important metal oxide; it is a nontoxic material with low cost and high stability at the surrounding state (Teja and Koh 2009). α-Fe_2O_3 is an antiferromagnetic material with n-type semiconductivity and a band gap of 2.73 eV (Kayani et al. 2015). α-Fe_2O_3 crystallinity is indicated by its color, namely blood red for fine crystals and black or gray for coarse crystals (Teja and Koh 2009).

Synthesized α-Fe$_2$O$_3$ materials are widely used in industrial and commercial applications, such as medicines (Gupta and Gupta 2005), Li-ion batteries (Zhang et al. 2010), anticorrosive agents (Palimi et al. 2015), adsorbent materials (Li et al. 2017; Hakim et al. 2016), gas sensors (Jadhav et al. 2013), chemical sensors (Umar et al. 2013), photocatalysts (Alagiri and Abd Hamid 2014; Ba-Abbad et al. 2016), and catalysts (Liu et al. 2007). Several methods, such as hydrothermal process (Zhang et al. 2012; Xu et al. 2011; Wang et al. 2009), direct thermal decomposition (Darezereshki et al. 2012), spin-coating technique (Navale et al. 2013), sol–gel (Alagiri and Abdul Hamid 2015; Liang et al. 2015), electrochemical anodization (Xie et al. 2014; Latempa et al. 2009), coprecipitation (Jacob and Khadar 2010; Lassoued et al. 2017), laser deposition technique (Thai et al. 2014), microwave synthesis (Hu et al. 2011), and microemulsion (Han et al. 2011), can be used to synthesize α-Fe$_2$O$_3$. In the present study, we modified and synthesized the composite of Fe/zeolite NPs via sol–gel method in the presence of polyethylene glycol (PEG) and oxalic acid. Sol–gel method is a simple and fast procedure that can be used in large-scale applications (Abdul Rahman et al. 2012).

Response surface methodology (RSM) is a combination of mathematical and statistical techniques with few experimental trials. RSM is used to design experiments and build models by setting various parameters to identify the optimum conditions for the desired responses (Pasma et al. 2013). RSM is extensively used in numerous fields, such as food science (Danbaba et al. 2015; Park et al. 2014), biotechnology (Singh and Sharma 2012), ester production (Mohamad Aziz et al. 2014), metal removal (Sharma et al. 2009), material development (Srikanth et al. 2016), leachate treatment (Abu Amr et al. 2014), color removal (Alkhatib et al. 2015), and bioprocessing (Pasma et al. 2013). Nevertheless, optimized parameters involved in Fe/zeolite NPs synthesis via sol–gel method based on a Box–Behnken design have yet to be used. Using Box–Behnken design can reduce the total number of runs, directly save time, and minimize the use of chemical substances. A Box–Behnken design can also decrease the entire cost and be used for a large number of factors in a single process (Jafarzadeh et al. 2011; Ba-Abbad et al. 2015). Therefore, Box–Behnken design and Doehlert matrix are slightly more efficient than central composite designs but are more efficient than three-level full factorial designs (Ferreira et al. 2007).

CO$_2$ concentration in the atmosphere increases with time and contributes to major problems, such as global warming, open burning, emission from vehicles, and industrial activity. To reduce CO$_2$ concentration, researchers extensively studied CO$_2$ hydrogenation in the presence of heterogeneous (Chiang et al. 2017) or homogeneous (Schneidewind et al. 2017) catalysts. Capturing and utilizing CO$_2$ into valuable products can be applied to decrease the CO$_2$ concentration in the atmosphere (Wan Isahak et al. 2015). An effective catalyst must be used in reactions because CO$_2$ is extremely thermodynamically stable for chemical transformation (Chiang et al. 2017). The application of a heterogeneous catalyst in CO$_2$ hydrogenation can play an important role and provide several advantages.

In this study, the conditions of Fe/zeolite nanocomposites as catalysts for the hydrogenation of CO$_2$ into formic acid were successfully synthesized and optimized. A Box–Behnken design was applied to optimize the properties (crystallite size) and to obtain the Fe/zeolite NPs using the optimum conditions. The effects and relationship of the synthesized parameters, such as weight ratio, volume of surfactant, and calcined temperature, were investigated, and the effect of crystal size on formic acid production was examined. Catalytic activity increases as the crystallite size decreases because of an increase in surface area (Carter et al. 1966). The amount of metal loading also affects the crystallite size, and an increased consumption of metal loading decreases the crystallite size (Bueno-Ferrer et al. 2010).

Materials and methods

Experimental

Preparation of a-Fe$_2$O$_3$ and composite Fe/zeolite NPs

α-Fe$_2$O$_3$ NPs were prepared via sol–gel method using Fe(III) nitrate nonahydrate (R&M Chemical), oxalic acid dihydrate (R&M Chemical), PEG 2000 (Merck), and absolute ethanol (HmbG Chemicals) as starting materials without any further purification. Fe(III) nitrate, as a reactant, was dissolved in absolute ethanol in a beaker and stirred with a magnetic stirrer at 60 ± 5 °C for 10 min. Then, small drops of PEG were added. Last, oxalic acid solution was slowly added to the mixture until its color changed to greenish, and the resulting mixture was stirred continuously for 30 min. Afterward, the solution was dried overnight in an oven at 105 °C. Then, further calcination at 400 °C was performed for 2 h.

Fe/zeolite was prepared via sol–gel method using the same materials as listed above, but zeolite 13× was added instead of oxalic acid solution (Fluka BioChemika). Absolute ethanol was added in a beaker containing zeolite as a reactant by stirring with a magnetic stirrer at 60 ± 5 °C for 10 min. Then, Fe(III) nitrate Fe(NO$_3$)$_3$·9H$_2$O was slowly added, and the resulting solution was continuously stirred for 10 min. Next, PEG was added dropwise. Oxalic acid with absolute ethanol was heated in another beaker by stirring with a magnetic stirrer until the solution became clear. Subsequently, gel was formed under vigorous magnetic conditions when oxalic acid solution was added to the previous beaker and stirred for 30 min. Afterward, the produced gel was dried overnight at 105 °C. Finally, brown powder was calcined using various selective temperatures for 2 h. Numerous process parameters,

such as weight ratio of a metal to a support material, PEG volume, and calcined temperature, were optimized. The parameters were selected on the basis of their effect on crystal size formation. A previous research showed that the ratio of a metal to a support can increase or decrease reactions (Díez-Ramírez et al. 2017), and PEG addition can control crystal size and improve particle morphology (Razavian et al. 2014). Moreover, the most important parameter is calcination temperature because it can increase the crystallinity of materials and remove any impurities present on the surface (Sifontes et al. 2013)(Xu et al. 2017).

CO_2 hydrogenation reaction

The activity and selectivity of the prepared Fe/zeolite NP catalyst for CO_2 hydrogenation were demonstrated in an autoclave reactor using 1,4-dioxane (Fisher Chemical), CO_2 (compressed, NIG Gases Sdn. Bhd.), and H_2 (compressed, purified gas from Linde Malaysia Sdn. Bhd.) without further purification. The reactor consisting of a stainless steel chamber (~ 12.3 cm in length and 6.5 cm in internal diameter) was placed in an electrically heated oven. The amount of Fe/zeolite NP catalyst in the experiments was constant at 0.2 g. Afterward, 35 mL of 1,4-dioxane was used as a solvent for the reactions, and H_2 flushing was performed for 1 min to remove air. Then, CO_2 and H_2 gases were filled to the desired pressure of 35 bar (initial pressure) at a ratio of 1:3 and heated to 130 °C. The mixture was stirred under these conditions for 6 h, which was the reaction time for all of the experiments.

Afterward, the reactor was left overnight to cool down to room temperature, and the pressure was slowly released. The concentration of the generated formic acid was analyzed using high-performance liquid chromatography (HPLC). The experimental setup for the reaction is illustrated in Fig. 1.

Orthogonal array and characterization methods

In this research, the weight ratio of Fe(III) nitrate (nonahydrate) to zeolite 13× (mass $Fe(NO_3)_3 \cdot 9H_2O$:mass zeolite) was diversified within the range of 25–100% at a constant zeolite mass of 2 g. PEG volume varied from 1 to 3 mL, and the calcined temperature varied from 400 to 600 °C. Their respective levels set to ensure the optimum conditions by applying all independent variable parameters are shown in Table 1. The crystal sizes and structures of Fe NPs and zeolite were analyzed using X-ray diffractometer (XRD, Bruker D8 Advance) with a CuKα radiation of 1.5046 Å in the 2θ scan ranging from 5° to 80°. The sizes and shapes of NPs

Table 1 Parameter and level for Box–Behnken design

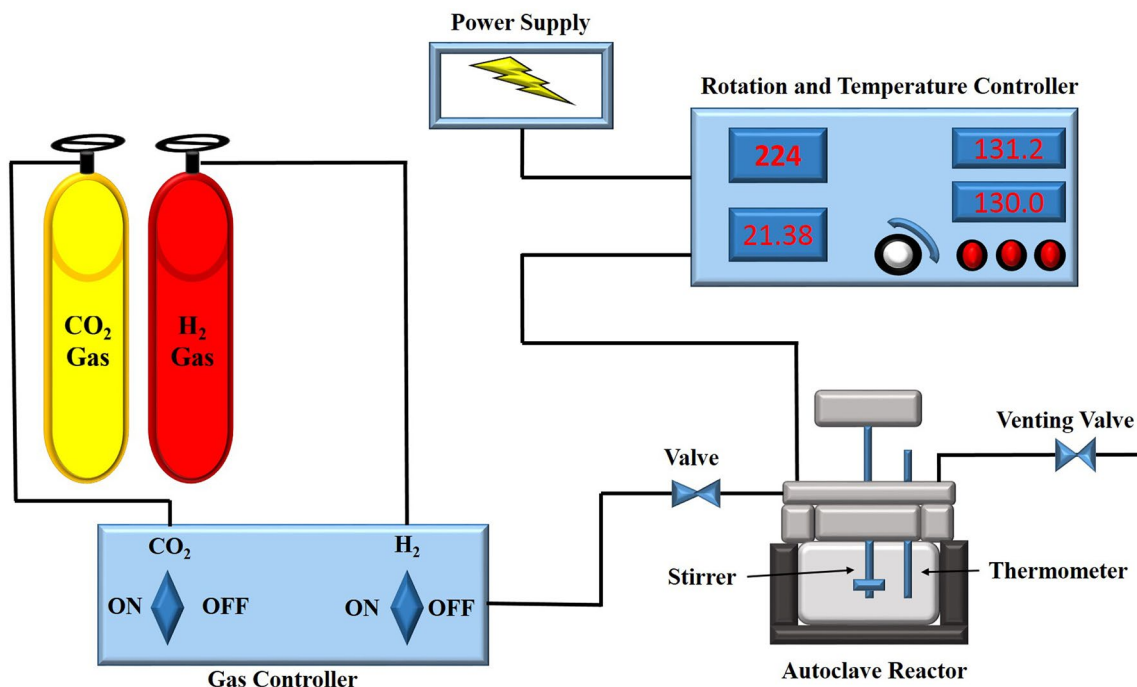| Independent variable parameters	Units	Factor X_i	Range and level		
			−1	0	+1
Weight ratio	%	X_1	25	62.5	100
The volume of PEG	mL	X_2	1	2	3
Calcined temperature	°C	X_3	400	500	600

Fig. 1 Experimental setup for CO_2 hydrogenation into formic acid

and Fe/zeolite nanocomposites were evaluated using a transmission electron microscope (TEM, Philip TEMCM12).

Experimental design and optimization

All of the prepared experiment designs for Fe/zeolite NPs were accomplished on the basis of the Box–Behnken design. In particular, the Box–Behnken design consisting of 17 experimental runs was used to determine the effects of each independent variable on the crystal size of Fe NPs. The independent variables, namely X_1, X_2, and X_3, represented the weight ratio [mass Fe(III) nitrate:mass zeolite], PEG volume (mL), and calcination temperature (°C), respectively. To specify all of the independent variables, we applied low and high values (Table 1). To predict the optimum point, we used either a linear model or a quadratic model to correlate the relationship between independent variables and response (i.e., crystal size of Fe). The equation for three factors is indicated below:

$$Y = \beta_o + \beta_1 x_1 + \beta_2 x_2 + \beta_3 x_3 + \beta_{12} x_1 x_2 + \beta_{13} x_1 x_3 \\ + \beta_{23} x_2 x_3 + \beta_{11} x_1^2 + \beta_{22} x_2^2 + \beta_{33} x_3^2, \tag{1}$$

where Y is the predicted response; β_o is the model's constant; x_1, x_2, and x_3 are the independent variables; x_1^2, x_2^2, and x_3^2 are the square effects; $x_1 x_2$, $x_1 x_3$, and $x_2 x_3$ are the interaction effects; β_1, β_2, and β_3 are the linear coefficients; β_{12}, β_{13}, and β_{23} are the interaction regression coefficients; and β_{11}, β_{22}, and β_{33} are the quadratic coefficients. The correlation of fitness for the regression model was expressed by the coefficient of determination of the normal regression (R^2) and adjusted regression (R_{adj}^2).

Results and discussion

To study the effect of the relationships between the independent variables on the crystal size of Fe/zeolite NPs through RSM based on a Box–Behnken design, several steps involved in the optimization of the design process were used, which completed the statistically designed experiment. ANOVA could explain the effects of interactions as shown in the experimental runs, and the adequacy of the model could be checked using a diagnostic graph. Last, responses should be predicted, and the model should be verified by testing the optimum experimental condition in accordance with the methods described by Zhang and Zheng (2009).

Model fitting of Box–Behnken design

The best model equation was obtained through the polynomial regression modeling that was operated among the response variables with the corresponding coded values of the three different variables (Singh et al. 2011). In the RSM involving the Box–Behnken design, 17 sets of experiments were carried out for the three selected factors with three levels. All of the responses of this design were generated

Table 2 Experimental runs of Box–Behnken design and response for Fe/zeolite nanoparticle production

Std	Run	Coded variables			Real variables			Crystal size (nm)	
		x_1	x_2	x_3	Weight ratio (X_1)	Volume of PEG (X_2)	Calcination temperature (X_3)	Experimental	Predicted
1	15	−1	−1	0	25	1	500	72.88	73.70
2	4	1	−1	0	100	1	500	43.24	44.77
3	11	−1	1	0	25	3	500	74.29	72.76
4	3	1	1	0	100	3	500	45.21	44.39
5	6	−1	0	−1	25	2	400	85.17	84.34
6	13	1	0	−1	100	2	400	41.18	39.64
7	5	−1	0	1	25	2	600	56.28	57.82
8	7	1	0	1	100	2	600	44.39	45.22
9	2	0	−1	−1	62.5	1	400	61.53	61.54
10	14	0	1	−1	62.5	3	400	57.96	60.31
11	10	0	−1	1	62.5	1	600	52.84	50.49
12	17	0	1	1	62.5	3	600	50.42	50.41
13	9	0	0	0	62.5	2	500	52.02	58.30
14	16	0	0	0	62.5	2	500	59.01	58.30
15	1	0	0	0	62.5	2	500	63.98	58.30
16	12	0	0	0	62.5	2	500	61.04	58.30
17	8	0	0	0	62.5	2	500	55.43	58.30

by each experiment, and the predicted values are listed in Table 2. The quadratic polynomial model was used to investigate the effect of independent variables on the size of Fe/zeolite nanocomposite as given by

$$Y = 58.30 - 14.32x_1 - 0.33x_2 - 5.24x_3 + 0.14x_1x_2 \\ + 8.03x_1x_3 + 0.29x_2x_3 + 0.84x_1^2 - 0.23x_2^2 - 2.38x_3^2.$$

(2)

Sen and Swaminathan (2004) considered the importance of testing the significance and adequacy of the model through ANOVA. The ANOVA results of the quadratic model are shown in Table 3. Segurola et al. (1999) showed that a model is statistically significant when P values are lower than 0.05. Conversely, when P values are greater than 0.1000, a model is insignificant. In our study, the model was significant because it had P and F values of 0.0009 and 15.03 (Table 3), respectively. The model also revealed that X_1, X_3, and X_{13} were significant ($P < 0.0001$, $P < 0.0075$, and $P < 0.0050$, respectively), with an adequate precision value of 14.630. Adequate precision measures the signal-to-noise ratio, and a ratio greater than 4 is desirable, indicating an adequate signal (Kayan and Gözmen 2012). Furthermore, the lack of fit (F value of 0.35) suggested that the lack of fit was insignificantly related to the pure error and benefited the model as reported previously (Zhang and Zheng 2009). The model yielded an R^2 of 0.9508 and an (R^2_{adj}) of 0.8875, confirming that the relationship between the regression model and the experimental values had a good fit (Ba-Abbad et al. 2013). The low Fe weight ratio to zeolite of 25% yielded a large crystal size of ~80 nm. The increase in the Fe-to-zeolite ratio of up to 100% led to a small nanoparticle size of

~42 nm. PEG volume and calcination temperature elicited a less significant effect than the weight ratio on the nanocomposite crystal size.

Adequacy check of the model

To ensure that the model accurately represented a real system, we should verify the model subjected to data analysis via an adequacy check analysis; otherwise, the model may give poor or misleading result (Körbahti and Rauf 2008). Equation (1) is used to visualize the effects of experimental factors on the degradation percentage response (Figs. 2, 3, 4, 5 and 6).

The normal probability percentage versus studentized residuals followed a normal distribution (Fig. 2). All of the
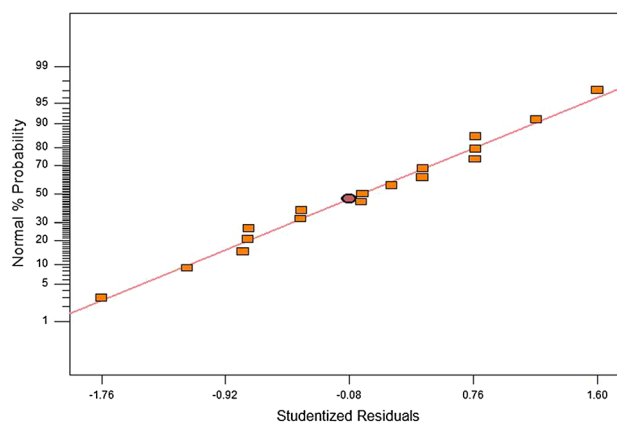

Fig. 2 The normal % probabilty versus studentized residuals for cystal size (nm) of Fe/zeolite nanoparticles

Table 3 ANOVA result for quadratic model of Fe/zeolite nanoparticle preparation

Source	Sum of squares	Degree of freedom	Mean square	F value	P value	Comments
Model	2146.47	9	238.50	15.03	0.0009	Significant
X_1	1641.64	1	1641.64	103.44	< 0.0001	
X_2	0.85	1	0.85	0.054	0.8234	
X_3	219.56	1	219.56	13.83	0.0075	
X_1^2	2.96	1	2.96	0.19	0.6789	
X_2^2	0.22	1	0.22	0.014	0.9093	
X_3^2	23.84	1	23.84	1.50	0.2600	
X_{12}	0.078	1	0.078	0.0049	0.9459	
X_{13}	257.60	1	257.60	16.23	0.0050	
X_{23}	0.33	1	0.33	0.021	0.8893	
Residual	111.09	7	15.87			
Lack of fit	23.15	3	7.72	0.35	0.7920	Not significant
Pure error	87.95	4	21.99			
Total	2257.56	16				

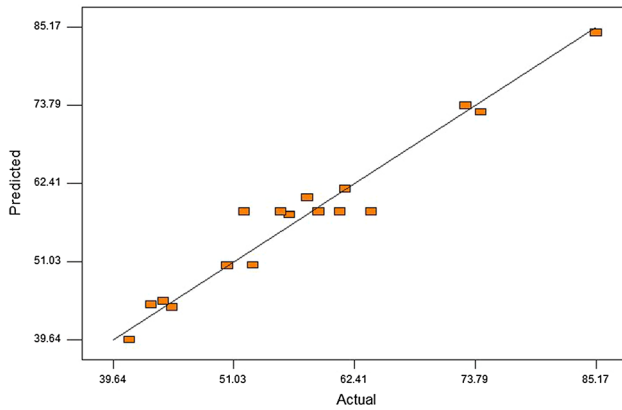$R2 = 0.9508$, $R^2_{adj} = 0.8875$, adequate precision = 14.630

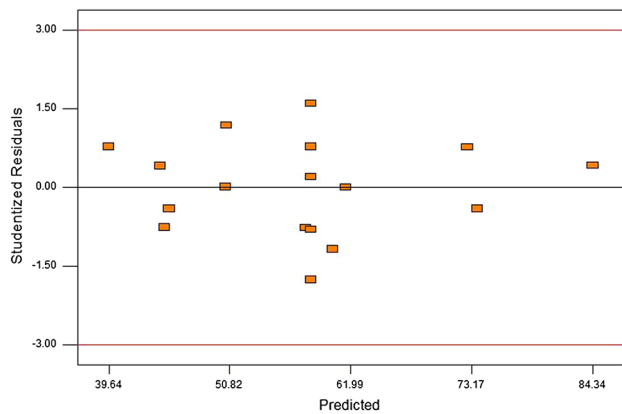**Fig. 3** Predicted versus actual crystal size (nm) of Fe/zeolite nanoparticles

Fig. 4 Residual versus predicted of crystal size (nm) of Fe/zeolite nanoparticles
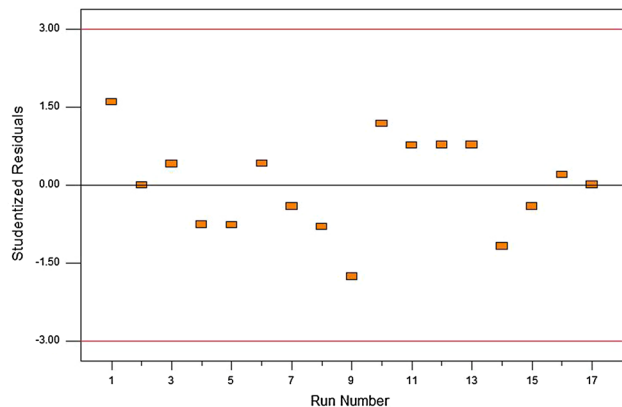

Fig. 5 Residuals versus run number for crystal size (nm) of Fe/zeolite nanoparticles

points followed a straight line for each case. Abu Amr et al. (2014) indicated that some scatterings are assumed as normal data that can be possibly considered as normally distributed in the responses of certain models.
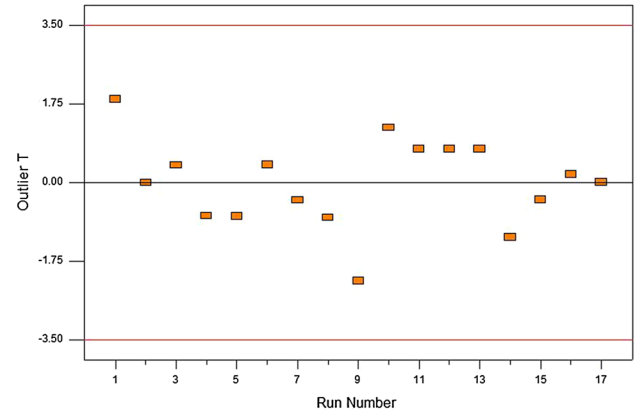

Fig. 6 Outlier T versus run number of crystal size (nm) for Fe/zeolite nanoparticles

Figure 3 shows the predicted size versus actual crystal size (nm) of Fe/zeolite NPs. The actual crystal size was acquired from the experiment, whereas the predicted crystal size was obtained from the calculation based on the model (Ba-Abbad et al. 2013). In Fig. 2, R^2 and R^2_{adj} were 0.9508 and 0.8875, respectively. A high R^2 did not confirm the goodness of fit of the regression model to determine the fit of the regression model based on R^2_{adj} (Zhang and Zheng 2009). In our study, R^2_{adj} was smaller than R^2 because many terms were present in the model, and the sample size was small (Singh et al. 2011). R^2 might be decreased by the insignificant terms listed in Table 3 (Ba-Abbad et al. 2013).

Figure 4 shows the plot of residuals against the predicted crystal size of Fe/zeolite NPs. No parameter was required to change the response variable because the plot of variance was randomly scattered. This result showed that the variance was constant for every response value. If the response variance depends mostly on the mean of the y-axis, then its plot is randomly scattered, regularly exhibiting a funnel-shaped pattern (Myers and Montgomery 2002). The plot of residuals against the run number of the crystal size was tested (Fig. 5), and the residuals were scattered randomly at approximately ± 3.00. Chowdhury et al. (2012) indicated that model and experimental data show a good fit.

The outlier T versus the run number of crystal size is shown in Fig. 6. All of the plots of the outliers were scattered randomly at approximately ± 3.50 and significantly different from those of the other cases. The outlier of the experimental runs significantly showed that these points had a good distribution for the Box–Behnken design. No outlier at approximately ± 3.50 was observed. If an outlier was present, then the experimental run should be repeated again until it reached the desired range.

Response surface plotting and optimization of crystal size

The influence of the interaction between the two variables was discussed in terms of the crystal size of Fe/zeolite NPs as 3D response surfaces and contour graphs. Response surfaces indicated the influences of the weight ratio of initial materials (Fe:zeolite) to the volume usage of PEG on the crystal size of Fe/zeolite NPs (Fig. 7). The crystal size of Fe/zeolite NP increased as the weight ratio decreased from

100 to 25%. An increase in size was generally due to crystal growth (Ba-Abbad et al. 2013). The crystal size remained constant as the PEG volume increased from 1 to 3 mL. Crystallinity and crystal size depend on the volume of surfactants (Dong et al. 2016) because the increased volume of surfactant increases the potential for agglomeration to occur (Ba-Abbad et al. 2017). Table 3 shows that the P value of the interaction effect between the weight ratio and PEG volume (X_1X_2) was insignificant (0.9459) to the model design because the value was above 0.05.

Fig. 7 **a** 3-D response surface **b** contour graph regarding the effect of the weight ratio and volume of PEG on the crystal size of Fe/zeolite nanoparticles
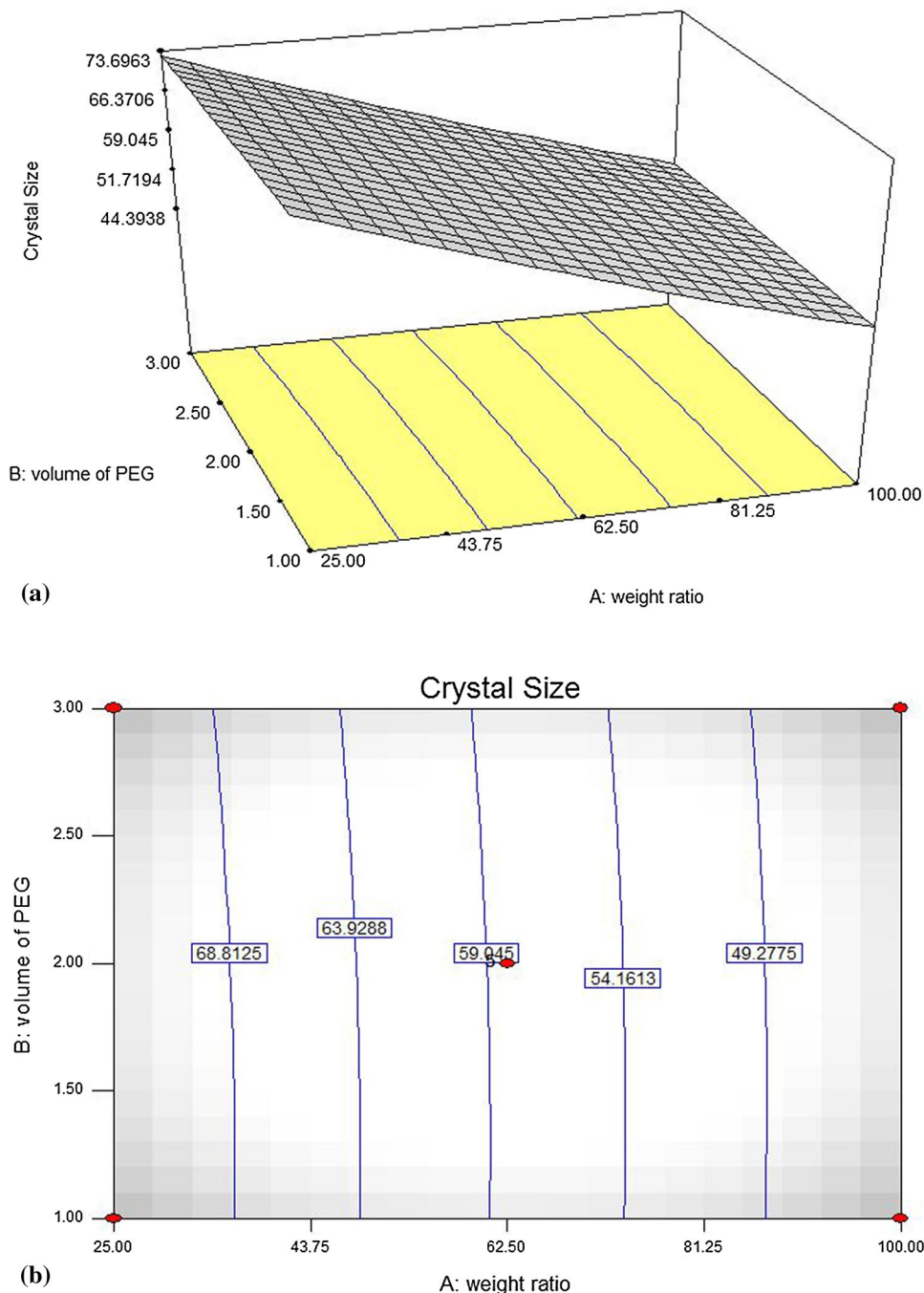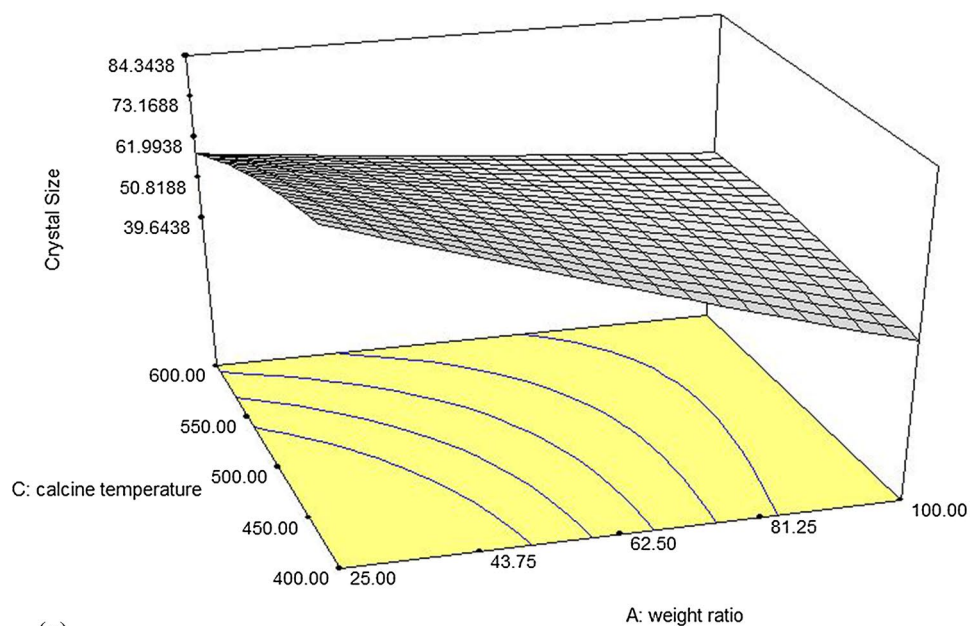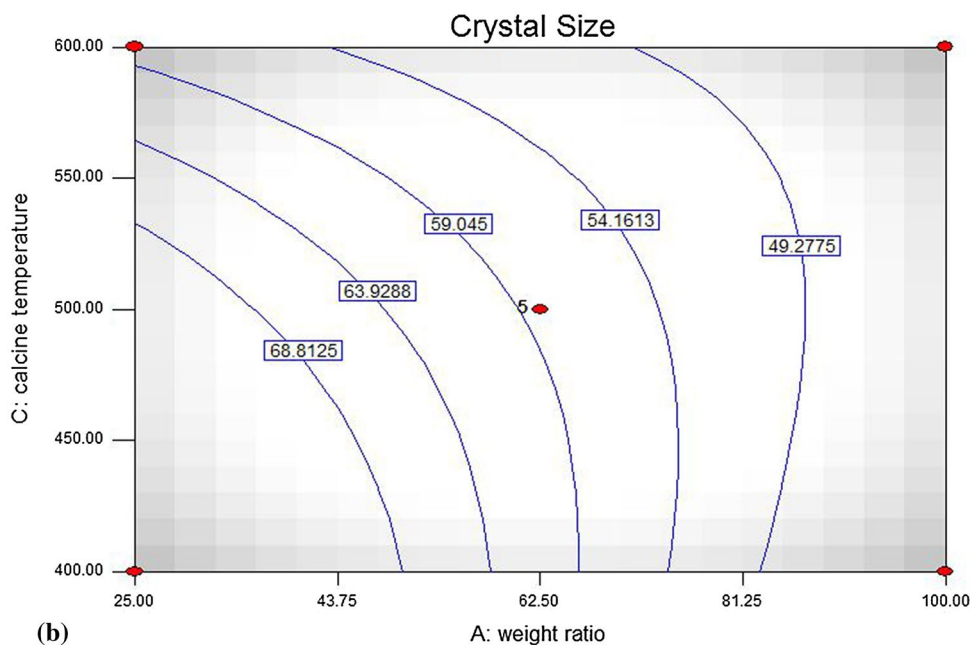
Fig. 8 **a** 3-D response surface **b** contour graph regarding the effect of the weight ratio and calcine temperature on the crystal size of Fe/zeolite nano-particles

(a)

(b)

The effects of weight ratio and calcination temperature on the crystal size of Fe/zeolite NPs were investigated (Fig. 8). The results showed that crystal size increased as the weight ratio decreased, confirming that a sufficient amount of reactants for a reaction plays a major role in controlling the final size of NPs (Ba-Abbad et al. 2015). Crystal size increased as the calcination temperature decreased from 600 to 400 °C. This result demonstrated the significant effect of calcination temperature on the final particle size because of the agglomeration of small particles during calcination to produce large particles (Ba-Abbad et al. 2015). In Table 3, the P value of the interaction effect between the weight

ratio and calcination temperature was significant (0.0050) to the model, thereby verifying that the factors had strong interaction.

Figure 9 shows the effects of PEG volume and calcination temperature on the crystal size of Fe/zeolite NPs. The crystal size of Fe/zeolite NPs increased as calcination temperature decreased from 600 to 400 °C. The crystal size of Fe/zeolite remained constant as the volume of PEG increased from 1 to 3 mL. These results indicated that particle size decreased as the volume of PEG used as a capping agent increased because of its effect on the nuclei and growth of NPs (Ba-Abbad et al. 2017). The

Fig. 9 **a** 3-D response surface **b** contour graph regarding the effect of the volume of PEG and calcine temperature on the crystal size of Fe/zeolite nanoparticles
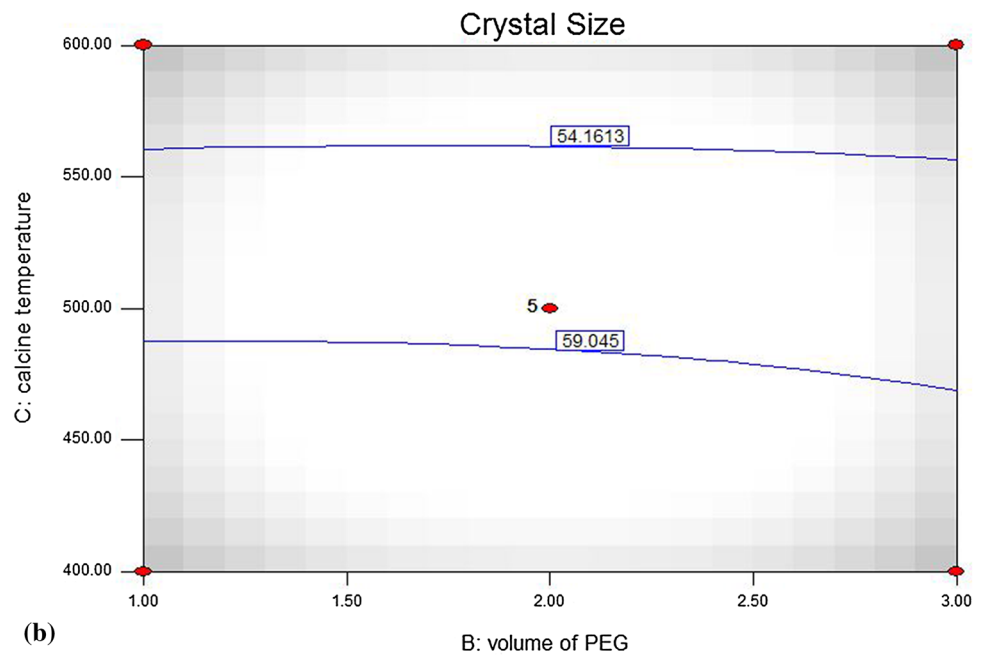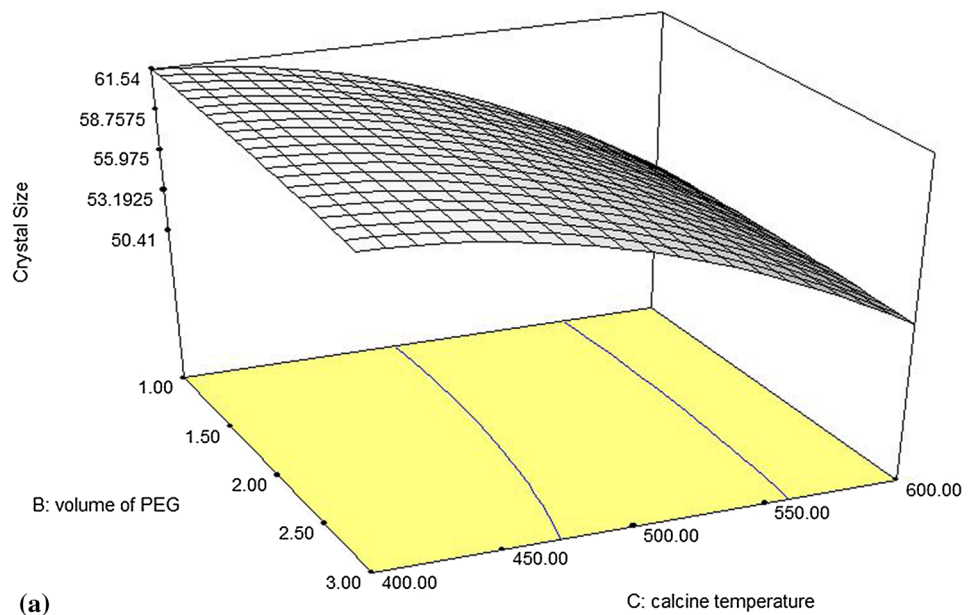

(a)

(b)

Table 4 Optimization of all factors

Parameter	Aim	Lower limit	Upper limit	Lower weight	Upper weight
Weight ratio	Is in range	25	100	1	1
Volume of PEG	Is in range	1	3	1	1
Calcination temperature	Is in range	400	600	1	1
Crystal size (nm)	Is in range	41.18	85.17	1	1

final particle size decreased as calcination temperature increased from 400 to 600 °C because a small particle size was produced as the volume of PEG increased. As calcination temperature increased, small particles were observed. This result was consistent with previous findings (Ba-Abbad et al. 2017). The *P* value of the interaction

between calcination temperature and PEG volume was insignificant (0.8893) to the model (Table 3). A weak interaction was observed as indicated by $P > 0.05$.

Model validation and experimental confirmation

The validity of the predicted model was investigated in terms of desirability function ($D = 1.000$) to determine the optimal conditions for the production of Fe/zeolite NPs. Table 4 shows the parameters that could be adjusted to none, maximum, minimum, target, within range, or equal to the optimization of Fe/zeolite NPs. In Fig. 10, the crystal size obtained from the DOE software was 52.5 nm. The following independent variables were also determined: weight ratio, PEG volume, and calcination temperature of 66.55%, 1.68 mL, and 570.58 °C, respectively. The experimental crystal size of Fe/zeolite NP by run 9 with a value of 52.02 nm was consistent with the results obtained from the optimization analysis by the DOE software.

Fig. 10 The crystal size as derived from the Box–Behnken design predicted the model using the optimal conditions
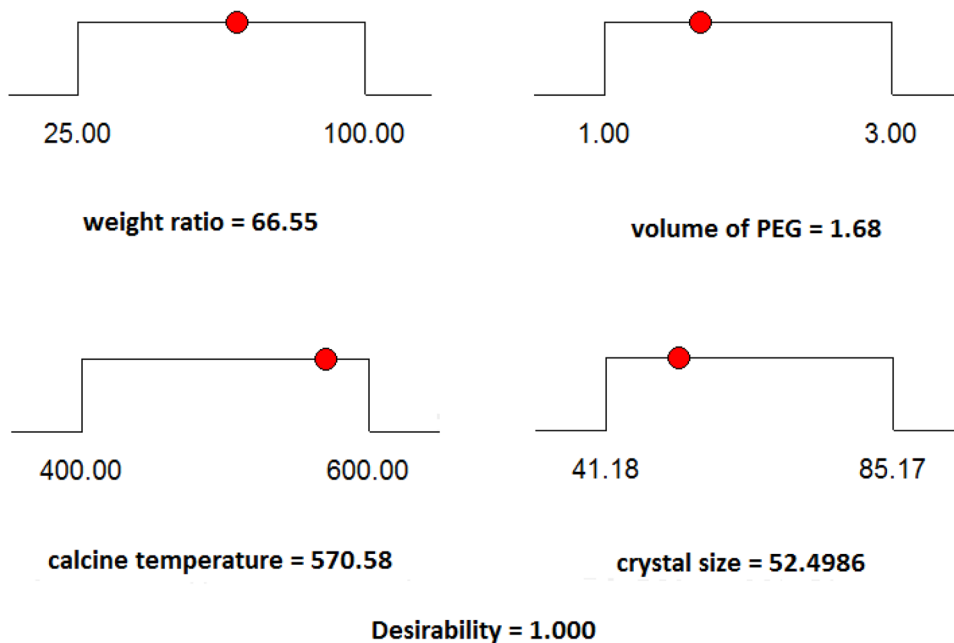

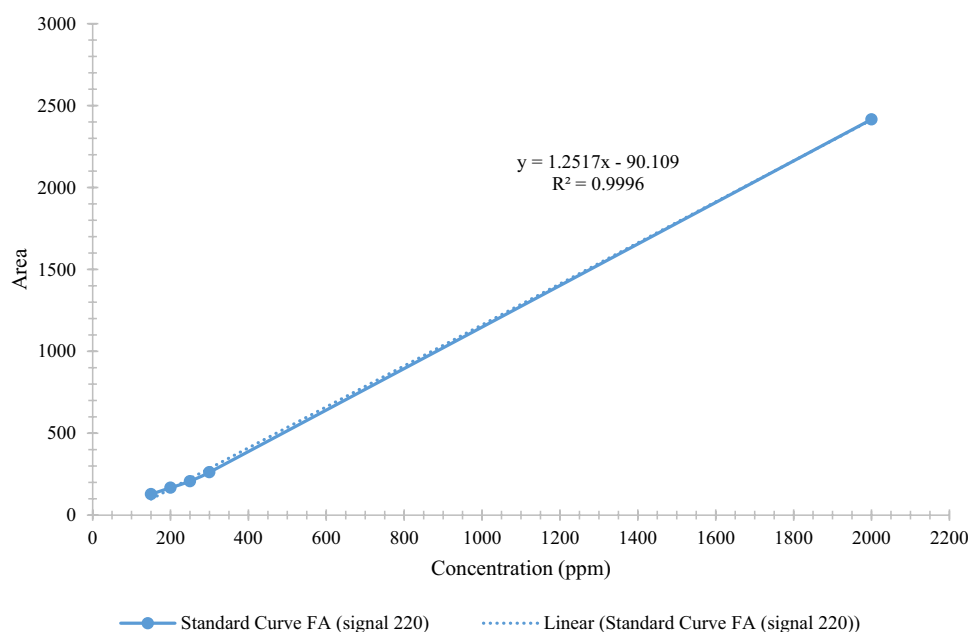**Fig. 11** Standard curve of formic acid (FA)

**Table 5** The production of formic acid (FA) through the CO_2 hydrogenation using Fe/zeolite catalyst

Run number	Crystal size (nm) (experimental)	Formic acid yield (ppm)
1	63.98	170.65
2	61.53	346.31
3	45.21	187.05
4	43.24	458.99
5	56.28	704.18
6	85.17	354.18
7	44.39	459.27
8	55.43	338.40
9	52.02	1131.63
10	52.84	342.18
11	74.29	305.22
12	61.04	481.15
13	41.18	242.56
14	57.96	105.84
15	72.88	203.19
16	59.01	187.01
17	50.42	170.63

Effect of crystal size on catalytic activity

The optimum conditions were determined through the formation of Fe/zeolite NPs between the crystal size (nm) related to formic acid production via CO_2 hydrogenation. Formic acid as the main product of CO_2 hydrogenation was analyzed through HPLC, and its standard curve is presented in Fig. 11. The condition for CO_2 hydrogenation was explained previously in the "Experimental" section. Table 5 shows the effects of the crystallite size of Fe/zeolite on producing a certain concentration of formic acid. Run 9 yielded the highest formic acid concentration (ppm or mg/L) of 1131.63 ppm. The highest formic acid concentration produced was found to be in the crystallite size of 52.02 nm, with the following independent variables: weight ratio of 62.5%, PEG volume of 2 mL, and calcination temperature of 500 °C. A previous research showed that small crystals with large surface area, pore volume, and pore diameter can enhance the diffusion rate of the reaction of products (Zhang et al. 2018).

Characterization of Fe/zeolite NPs

To support the findings of the optimized parameters of sol–gel method and CO_2 hydrogenation performance, we characterized Fe NPs and their composite with zeolite through XRD and TEM to study their crystallinity properties, shape, and particle sizes. The XRD data matched with
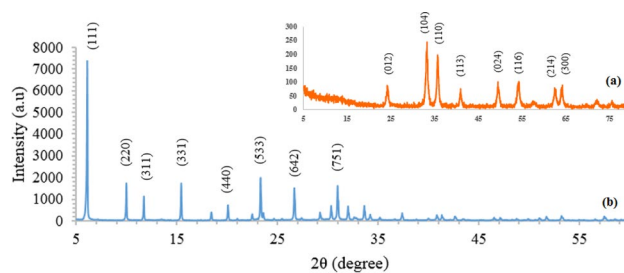
Fig. 12 X-ray pattern **a** α-Fe_2O_3, **b** zeolite 13×

the standard peak data reported by the Joint Committee on Powder Diffraction Standard (JCPDS) to identify the sample. These properties influenced the catalytic activities of Fe NPs and their composite with zeolite in CO_2 hydrogenation.

XRD analysis

The XRD patterns of α-Fe_2O_3, zeolite, and Fe/zeolite composite without any detectable impurities are shown in Figs. 12a, b, and 13, respectively. The rhombohedral hematite (α-Fe_2O_3) system had lattice parameters of $a = 0.53850$ nm and $c = 1.374$ nm (space group R-3C). The characteristic 2θ peaks at 24.1°, 33.1°, 35.6°, 40.8°, 49.4°, 54.0°, 62.4°, and 63.9° corresponded to (012), (104), (110), (113), (024), (116), (214), and (300) planes, respectively. These results matched well with JCPDS 071-5088.

Cubic zeolite had a lattice parameter of $a = 2.4973$ nm (space group Fd-3m). The characteristic 2θ peaks at 6.1°, 10.0°, 11.7°, 15.4°, 18.4°, 23.3°, 26.6°, and 30.9° corresponded to (111), (220), (311), (331), (440), (533), (642), and (751) planes, respectively. These results matched well with JCPDS 026-0893. Figure 12b shows the crystalline phase structure patterns of zeolite 13× (pure) while the Fe weight ratios of 25% Fe/zeolite, 62.5% Fe/zeolite, and 100% Fe/zeolite is shown in Fig. 13. The peak intensity of zeolite decreased as the Fe weight ratio increased, thereby indicating that zeolite 13× modification destroyed the framework. The interplanar spacing (d) and the average crystallite size of α-Fe_2O_3, zeolite, and composite Fe/zeolite were computed using Bragg's and Debye–Scherrer's formulas as indicated below, respectively:

$$d = \frac{\lambda}{2\sin\theta}, \tag{3}$$

$$D = \frac{K\lambda}{\beta\cos\theta}, \tag{4}$$

where D is the crystal size (nm or Å); K is the Scherrer constant ($K = 0.89$); λ is the X-ray wavelength (1.5406 Å) in the 2θ scan ranging from 5° to 80°; β is the peak width of half maximum; θ is the Bragg diffraction angle; and d is the
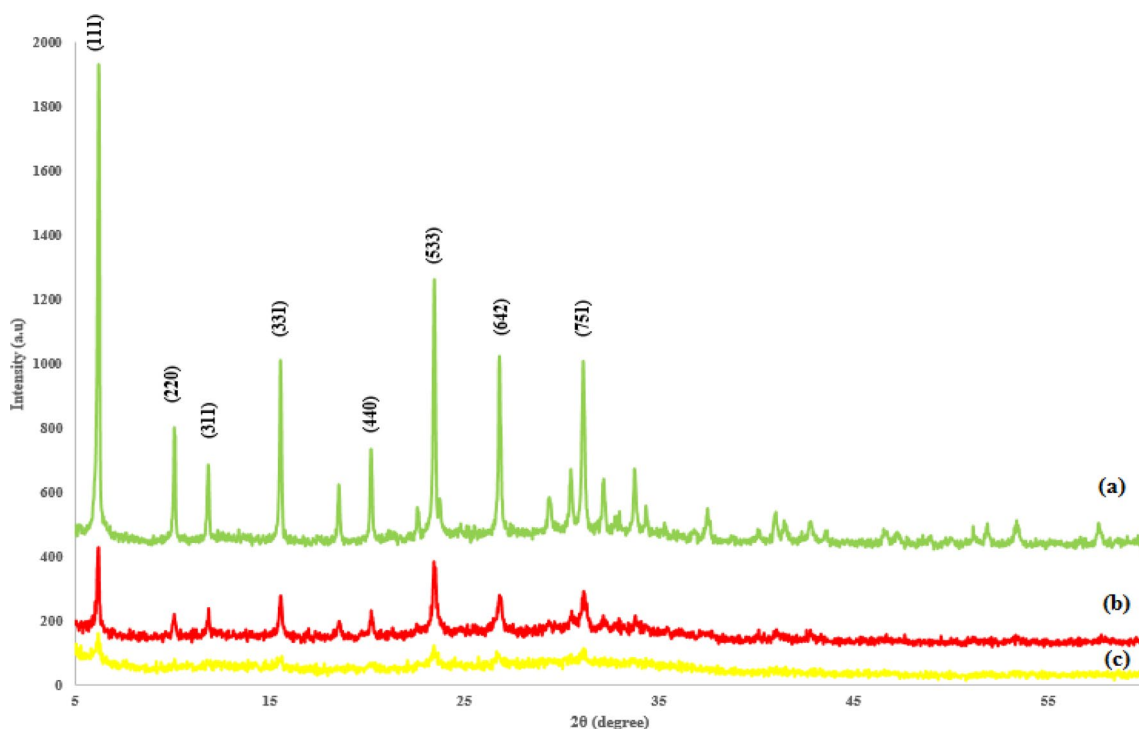
Fig. 13 X-ray pattern of Fe/zeolite composite: **a** Run 5, **b** Run 9 and **c** Run 13

Table 6 Interplanar spacing and intensity of α-Fe$_2$O$_3$ and zeolite nanoparticle peaks

h	k	l	2θ	α-Fe$_2$O$_3$			h	k	l	2θ	Zeolite		
				Intensity	d_{meas}	d_{cal}					Intensity	d_{meas}	d_{cal}
0	1	2	24.1	84.6	3.683	3.689	1	1	1	6.1	7439.0	14.418	14.477
1	0	4	33.1	244.0	2.699	2.704	2	2	0	10.0	1754.0	8.829	8.838
1	1	0	35.6	198.0	2.519	2.519	3	1	1	11.7	1140.0	7.529	7.557
1	1	3	40.8	75.1	2.207	2.209	3	3	1	15.4	1741.0	5.729	5.749
0	2	4	49.4	101.0	1.841	1.843	4	4	0	20.0	697.0	4.414	4.435
1	1	6	54.0	101.0	1.694	1.696	5	3	3	23.3	2006.0	3.808	3.814
2	1	4	62.4	76.9	1.486	1.486	6	4	2	26.6	1612.0	3.337	3.348
3	0	0	63.9	88.2	1.454	1.455	7	5	1	30.9	1635.0	2.883	2.891

Table 7 Interplanar spacing and intensity of Fe/zeolite nanoparticle peaks

| h	k	l	2θ	Run 5 (25% iron on zeolite)			h	k	l	2θ	Run 9 (62.5% iron on zeolite)			h	k	l	2θ	Run 13 (100% iron on zeolite)		
				Intensity	d_{meas}	d_{cal}					Intensity	d_{meas}	d_{cal}					Intensity	d_{meas}	d_{cal}
1	1	1	6.1	1528.0	14.30	14.48	1	1	1	6.2	329.0	14.27	14.24	1	1	1	6.2	163.0	14.272	14.244
2	2	0	10.0	380.0	8.76	8.84	2	2	0	10.1	123.0	8.74	8.75	2	2	0	NA	NA	NA	NA
3	1	1	11.8	238.0	7.47	7.49	3	1	1	11.8	141.0	7.45	7.49	3	1	1	NA	NA	NA	NA
3	3	1	15.5	607.0	5.68	5.71	3	3	1	15.5	177.0	5.67	5.71	3	3	1	NA	NA	NA	NA
4	4	0	20.2	273.0	4.38	4.39	4	4	0	20.2	134.0	4.37	4.39	4	4	0	NA	NA	NA	NA
5	3	3	23.5	861.0	3.78	3.78	5	3	3	23.4	286.0	3.77	3.80	5	3	3	23.4	125.0	3.77	3.80
6	4	2	26.9	601.0	3.31	3.31	6	4	2	26.8	176.0	3.30	3.32	6	4	2	26.6	106.0	3.34	3.35
7	5	1	31.2	562.0	2.86	2.86	7	5	1	31.1	186.0	2.85	2.87	7	5	1	31.2	110.0	2.86	2.86

NA not appear
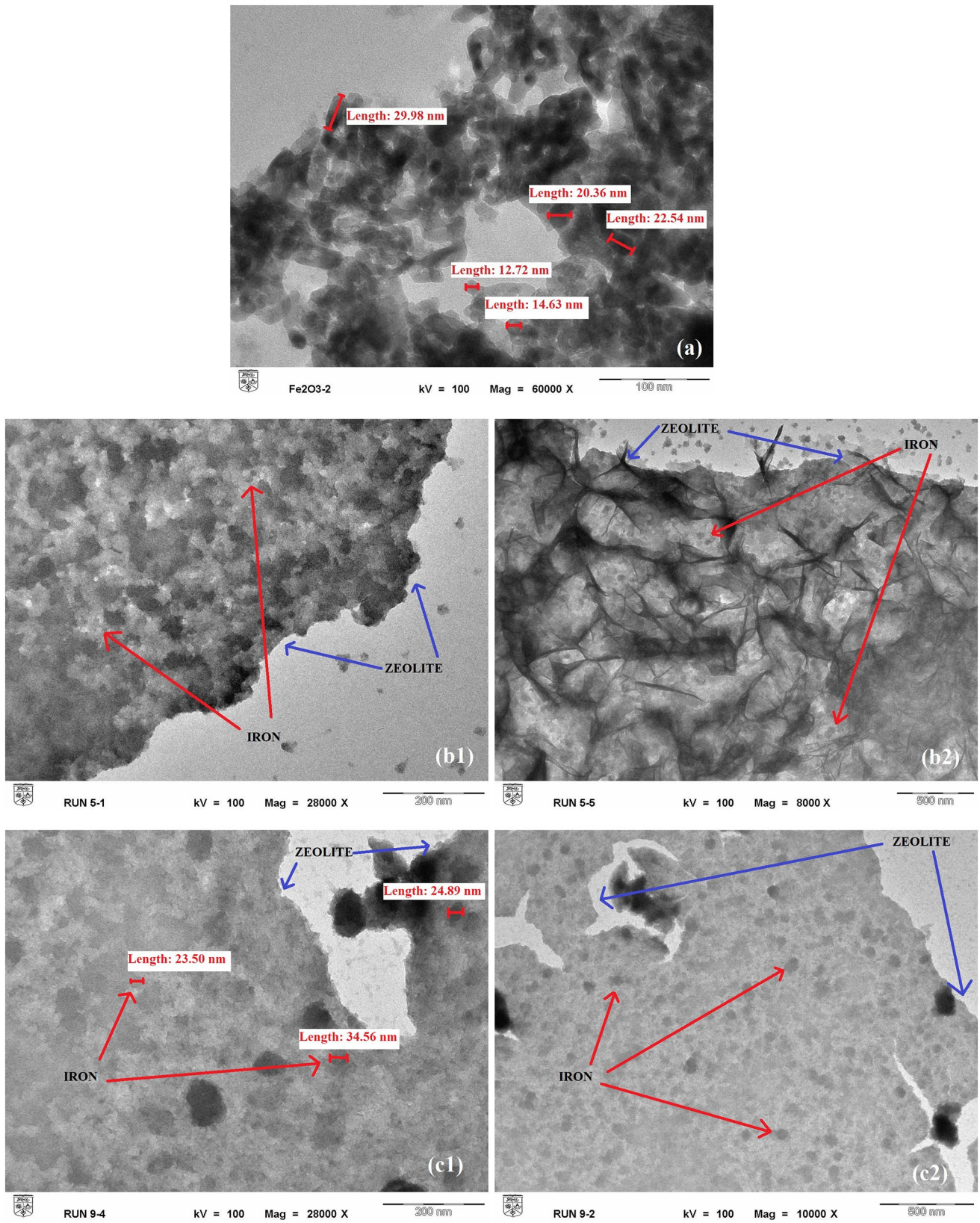
Fig. 14 The TEM image nanoparticles **a** pure Fe$_2$O$_3$ Nano. **b1, b2** Run 5 with 25% of Fe. **c1, c2** Run 9 with 62.5% of Fe

interplanar spacing. *d* and intensity values are summarized in Table 6 for α-Fe$_2$O$_3$ and zeolite peaks. The summarized data of the composite Fe/zeolite NPs are shown in Table 7. The similar structure phase indicated that the measured *d* from XRD was close to d calculated using Eq. (3) (Ba-Abbad et al. 2016).

Thus, all of the intensities of zeolite peaks decreased as the Fe ratio increased, confirming that Fe was consistent with the zeolite surface to make it an effective reaction site. After Fe was incorporated into zeolite, the *d* spacing of zeolite was not affected, suggesting that the value slightly changed (Tables 6, 7). As the main objective of this study, controlling the particle size of Fe on the zeolite surface was investigated to produce a high formic acid concentration from CO$_2$ hydrogenation under the optimum conditions for catalyst preparation (Carter et al. 1966).

Surface morphology

The effects of process parameters, such as weight ratio, PEG volume, and calcination temperature, on the morphological characteristics were studied. The particle size of Fe/zeolite NPs was evaluated through TEM under different magnifications. The surface morphology of the optimized sample, that is, run 9, with the highest formic acid concentration was analyzed through TEM and compared with that of run 5 prepared under different experimental conditions. The effects of these conditions, such as the weight ratio of the starting materials, PEG volume, and calcination temperature were observed. Figure 14a–c shows that pure Fe$_2$O$_3$ NP was quasi-spherical, whereas Fe$_2$O$_3$ NPs synthesized on the zeolite surface became a support layer (spherical), and the particle agglomeration increased. Pure quasispherical α-Fe$_2$O$_3$ NPs in the range of 12–22 nm were observed. However, the results showed large particle sizes ranging from 40 to 60 nm for the sample of Fe$_2$O$_3$–zeolite nanocomposite. This value was consistent with the values obtained from XRD analyses. The small particles agglomerated on the zeolite surface forming large particles, and the XRD results indicated that the size of these crystallites was 50 nm. The agglomeration of the particles on the zeolite surface was not uniform because of the effect of Fe weight ratio.

Figure 14b1, b2 illustrates that a layer was formed on zeolite that was not fully covered by Fe NPs because of the use of the low Fe weight ratio of 25% on zeolite. Figure 14b2 clearly shows the zeolite structure itself because the surface was not covered by Fe. Chen et al. (2016) showed that zeolite 13X has an octahedral structure that is nearly orbicular in appearance. However, at a high Fe weight ratio of 62.5% in run 9, the zeolite surface was completely covered by Fe NP. Thus, small particles agglomerated to each other (Fig. 14c1, c2). This ratio resulted in a high activity of the zeolite surface for the reaction to produce several formic

acids because of the balance between the surface areas of zeolite to the Fe weight ratio (Ba-Abbad et al. 2015; Chen et al. 2016). Therefore, a high Fe weight ratio (100 wt%) favored the formation of low formic acid concentration possibly because Fe NPs fully covered the zeolite surface, thereby resulting in a thick layer.

Conclusion

The synthesis of Fe/zeolite NPs through sol–gel method was optimized using a Box–Behnken design to produce formic acid. The effects of independent variables and their interactions on crystal size were also examined. ANOVA results showed that the predicted results were consistent with the experimental results. The correlation coefficients of R^2 and R^2_{adj} were 0.9508 and 0.8875, respectively. The optimized nanocomposite system could produce the highest formic acid concentration of 1131.63 ppm under the following optimum conditions: Fe/zeolite weight ratio of 62.5%, PEG volume of 2 mL, and calcination temperature of 500 °C. Crystal size influenced formic acid production through CO$_2$ hydrogenation at the reaction temperature and pressure of 130 °C and 35 bar, respectively. The experimental Fe/zeolite NP crystal size was 52.02 nm, which agreed with the predicted value of 58.30 nm, and it could produce the highest formic acid concentration. Thus, Fe/zeolite NP provided the compulsory support in the validation of the model and RSM based on the Box–Behnken design as an appropriate tool to optimize the conditions of formic acid production. The controllable crystallite size of Fe/zeolite NPs played a major role in obtaining the most efficient nanocomposite system of Fe/zeolite as a catalyst in the conversion of CO$_2$ into formic acid. Thus, Fe/zeolite NPs showed potential as a H$_2$ storage material.

Compliance with ethical standards

Conflict of interest The authors declare that they have no conflict of interest.

References

Abdul Rahman NA, Mustaffa NA, Abdul Aziz ND, Badar N, Kamarulzaman N (2012) Synthesis and characterization of Fe$_2$O$_3$ prepared via sol–gel method. Adv Mater Res 545:410–413. https://doi.org/10.4028/www.scientific.net/AMR.545.410

Abu Amr SS, Abdul Aziz H, Bashir MJK (2014) Application of response surface methodology (RSM) for optimization of

semi-aerobic landfill leachate treatment using ozone. Appl Water Sci 4:231–239. https://doi.org/10.1007/s13201-014-0156-z

Alagiri M, Abd Hamid SB (2014) Synthesis, characterization and photocatalytic application of α-Fe₂O₃ microflower. Mater Lett 136:329–332. https://doi.org/10.1016/j.poly.2011.11.017

Alagiri M, Abdul Hamid SB (2015) Sol-gel synthesis of α-Fe₂O₃ nanoparticles and its photocatalytic application. J Sol Gel Sci Technol 74:783–789. https://doi.org/10.1007/s10971-015-3663-y

Alkhatib MF, Mamun AA, Akbar I (2015) Application of response surface methodology (RSM) for optimization of color removal from POME by granular activated carbon. Int J Environ Sci Technol 12:1295–1302. https://doi.org/10.1007/s13762-014-0504-4

Ba-Abbad MM, Kadhum AAH, Mohamad AB, Takriff MS, Sopian K (2013) Optimization of process parameters using D-optimal design for synthesis of ZnO nanoparticles via sol–gel technique. J Ind Eng Chem 19:99–105. https://doi.org/10.1016/j.jiec.2012.07.010

Ba-Abbad MM, Chai PV, Takriff MS, Benamor A, Mohammad AW (2015) Optimization of nickel oxide nanoparticle synthesis through the sol–gel method using Box–Behnken design. Mater Des 86:948–956. https://doi.org/10.1016/j.matdes.2015.07.176

Ba-Abbad MM, Takriff MS, Benamor A, Mohammad AW (2016) Size and shape controlled of alpha-Fe₂O₃ nanoparticles prepared via sol–gel technique and their photocatalytic activity. J Sol Gel Sci Technol 1–14. https://doi.org/10.1007/s10971-016-4228-4

Ba-Abbad MM, Takriff MS, Benamor A, Mahmoudi E, Mohammad AW (2017) Arabic gum as green agent for ZnO nanoparticles synthesis: properties, mechanism and antibacterial activity. J Mater Sci Mater Electron 28:12100–12107. https://doi.org/10.1007/s10854-017-7023-2

Bueno-Ferrer C, Parres-Esclapez S, Lozano-Castelló D, Bueno-López A (2010) Relationship between surface area and crystal size of pure and doped cerium oxides. J Rare Earths 28:647–653. https://doi.org/10.1016/S1002-0721(09)60172-1

Carter JL, Cusumano JA, Sinfelt JH (1966) Catalysis over supported metals. V. The effect of crystallite size on the catalytic activity of nickel. J Phys Chem 70:2257–2263. https://doi.org/10.1021/j100879a029

Chen SJ, Fu Y, Huang YX, Tao ZC, Zhu M (2016) Experimental investigation of CO₂ separation by adsorption methods in natural gas purification. Appl Energy 179:329–337. https://doi.org/10.1016/j.apenergy.2016.06.146

Chiang CL, Lin KS, Chuang HW, Wu CM (2017) Conversion of hydrogen/carbon dioxide into formic acid and methanol over Cu/CuCr₂O₄ catalyst. Int J Hydrogen Energy. https://doi.org/10.1016/j.ijhydene.2017.04.226

Chowdhury ZZ, Zain SM, Khan RA, Ahmad AA, Khalid K (2012) Application of response surface methodology (RSM) for optimizing production condition for removal of Pb (II) and Cu (II) onto Kenaf fiber based activated carbon. Appl Sci Eng Technol 4:458–465

Danbaba N, Nkama I, Badau MH (2015) Application of response surface methodology (rsm) and central composite design (CCD) to optimize minerals composition of rice-cowpea composite blends during extrusion cooking. Int J Food Sci Nutr Eng 5:40–52. https://doi.org/10.5923/j.food.20150501.06

Darezereshki E, Bakhtiari F, Alizadeh M, Behrad vakylabad A, Ranjbar M (2012) Direct thermal decomposition synthesis and characterization of hematite (α-Fe₂O₃) nanoparticles. Mater Sci Semicond Process 15:91–97. https://doi.org/10.1016/j.mssp.2011.09.009

Díez-Ramírez J, Dorado F, de la Osa AR, Valverde JL, Sánchez P (2017) Hydrogenation of CO₂ to methanol at atmospheric pressure over Cu/ZnO catalysts: influence of the calcination, reduction,

and metal loading. Ind Eng Chem Res. https://doi.org/10.1021/acs.iecr.6b04662

Dong Y, Chang Y, Wang Q, Tong J, Zhou J (2016) Effects of surfactants on size and structure of amylose nanoparticles prepared by precipitation. Bull Mater Sci 39:35–39. https://doi.org/10.1007/s12034-015-1115-5

Ferreira SLC, Bruns RE, Ferreira HS, Matos GD, David JM, Brandão GC, da Silva EGP, Portugal LA, dos Reis PS, Souza AS, dos Santos WNL (2007) Box–Behnken design: an alternative for the optimization of analytical methods. Anal Chim Acta 597:179–186. https://doi.org/10.1016/j.aca.2007.07.011

Gupta AK, Gupta M (2005) Synthesis and surface engineering of iron oxide nanoparticles for biomedical applications. Biomaterials 26:3995–4021. https://doi.org/10.1016/j.biomaterials.2004.10.012

Hakim A, Marliza TS, Abu Tahari NM, Wan Isahak RWN, Yusop RM, Mohamed Hisham WM, Yarmo AM (2016) Studies on CO₂ adsorption and desorption properties from various types of iron oxides (FeO, Fe₂O₃, and Fe₃O₄). Ind Eng Chem Res 55:7888–7897. https://doi.org/10.1021/acs.iecr.5b04091

Han L, Liu H, Wei Y (2011) In situ synthesis of hematite nanoparticles using a low-temperature microemulsion method. Powder Technol 207:42–46. https://doi.org/10.1016/j.powtec.2010.10.008

Hu L, Percheron A, Chaumont D, Brachais CH (2011) Microwave-assisted one-step hydrothermal synthesis of pure iron oxide nanoparticles: magnetite, maghemite and hematite. J Sol Gel Sci Technol 60:198–205. https://doi.org/10.1007/s10971-011-2579-4

Jacob J, Khadar MA (2010) VSM and Mossbauer study of nanostructured hematite. J Magn Magn Mater 322:614–621. https://doi.org/10.1016/j.jmmm.2009.10.025

Jadhav VV, Patil SA, Shinde DV, Waghmare SD, Zate MK, Mane RS, Han SH (2013) Hematite nanostructures: morphology-mediated liquefied petroleum gas sensors. Sens Actuators B Chem 188:669–674. https://doi.org/10.1016/j.snb.2013.07.072

Jafarzadeh NK, Sharifnia S, Hosseini SN, Rahimpour F (2011) Statistical optimization of process conditions for photocatalytic degradation of phenol with immobilization of nano TiO₂ on perlite granules. Korean J Chem Eng 28:531–538. https://doi.org/10.1007/s11814-010-0355-8

Kayan B, Gözmen B (2012) Degradation of Acid Red 274 using H₂O₂ in subcritical water: application of response surface methodology. J Hazard Mater 201–202:100–106. https://doi.org/10.1016/j.jhazmat.2011.11.045

Kayani ZN, Afzal A, Butt MZ, Batool I, Arshad S, Ali Y, Riaz S, Naseem S (2015) Structural, optical and magnetic properties of iron oxide nano-particles. Mater Today Proc 2:5660–5663. https://doi.org/10.1016/j.matpr.2015.11.105

Körbahti BK, Rauf MA (2008) Application of response surface analysis to the photolytic degradation of Basic Red 2 dye. Chem Eng J 138:166–171. https://doi.org/10.1016/j.cej.2007.06.016

Lassoued A, Dkhil B, Gadri A, Ammar S (2017) Control of the shape and size of iron oxide (α-Fe₂O₃) nanoparticles synthesized through the chemical precipitation method. Results Phys 7:3007–3015. https://doi.org/10.1016/j.rinp.2017.07.066

Latempa TJ, Feng X, Paulose M, Grimes CA (2009) Temperature-dependent growth of self-assembled hematite (α-Fe₂O₃) nanotube arrays: rapid electrochemical synthesis and photoelectrochemical properties. J Phys Chem 113:16293–16298

Li X, Liu Y, Zhang C, Wen T, Zhuang L, Wang X, Song G, Chen D, Ai Y, Hayat T, Wang X (2017) Porous Fe₂O₃ microcubes derived from metal organic frameworks for efficient elimination of organic pollutants and heavy metal ions. Chem Eng J. https://doi.org/10.1016/j.cej.2017.11.188

Liang H, Liu K, Ni Y (2015) Synthesis of mesoporous α-Fe₂O₃ via sol–gel methods using cellulose nano-crystals (CNC) as template

and its photo-catalytic properties. Mater Lett 159:218–220. https://doi.org/10.1016/j.matlet.2015.06.103

Liu CY, Chen CF, Leu JP, Lin YC (2007) Iron oxide nanoparticles within the pore system of mesoporous SBA-15 in different acidity: the synthesis and characterization. J Sol Gel Sci Technol 43:47–51. https://doi.org/10.1007/s10971-007-1534-x

Mohamad Aziz NA, Yunus R, Rashid U, Muhammad Syam A (2014) Application of response surface methodology (RSM) for optimizing the palm-based pentaerythritol ester synthesis. Ind Crops Prod 62:305–312. https://doi.org/10.1016/j.indcrop.2014.08.040

Myers RH, Montgomery DC (2002) Response surface methodology: process and product optimization using designed experiments, 3rd edn. Wiley, Hoboken. https://doi.org/10.1016/S0378-3758(97)81631-X

Navale ST, Bandgar DK, Nalge SR, Mulik RN, Pawar SA, Chougule MA, Patil VB (2013) Novel process for synthesis of α-Fe$_2$O$_3$: microstructural and optoelectronic investigations. J Mater Sci Mater Electron 24:1422–1430. https://doi.org/10.1007/s10854-012-0944-x

Palimi MJ, Rostami M, Mahdavian M, Ramezanzadeh B (2015) A study on the corrosion inhibition properties of silane-modified Fe$_2$O$_3$ nanoparticle on mild steel and its effect on the anticorrosion properties of the polyurethane coating. J Coat Technol Res 12:277–292. https://doi.org/10.1007/s11998-014-9631-6

Park SY, Cho SA, Lim SD (2014) Application of response surface methodology (RSM) for optimization of anti-obesity effect in fermented milk by lactobacillus plantarum Q180. Korean J Food Sci An 34:836–843. https://doi.org/10.5851/kosfa.2014.34.6.836

Pasma SA, Daik R, Maskat MY, Hassan O (2013) Application of Box–Behnken design in optimization of glucose production from oil palm empty fruit bunch cellulose. Int J Poly Sci. https://doi.org/10.1155/2013/104502

Razavian M, Fatemi S, Komasi M (2014) Investigation the role of polyethylene glycol (PEG) as a co-template in synthesis of SAPO-34 catalyst. In: Proceedings of the the 8th international chemical engineering congress & exhibition, Kish, Iran, 24–27 February 2017

Schneidewind J, Adam R, Baumann W, Jackstell R, Beller M (2017) Low-temperature hydrogenation of carbon dioxide to methanol with a homogeneous cobalt catalyst. Angew Chem 56:1–5. https://doi.org/10.1002/ANGE.201609077

Segurola J, Allen NS, Edge M, Mc Mahon A (1999) Design of eutectic photoinitiator blends for UV/visible curable acrylated printing inks and coatings. Prog Org Coat 37:23–37. https://doi.org/10.1016/S0300-9440(99)00052-1

Sen R, Swaminathan T (2004) Response surface modeling and optimization to elucidate and analyze the effects of inoculum age and size on surfactin production. Biochem Eng J 21:141–148. https://doi.org/10.1016/j.bej.2004.06.006

Sharma S, Malik A, Satya S (2009) Application of response surface methodology (RSM) for optimization of nutrient supplementation for Cr (VI) removal by *Aspergillus lentulus* AML05. J Hazard Mater 164:1198–1204. https://doi.org/10.1016/j.jhazmat.2008.09.030

Sifontes AB, Rosales M, Méndez FJ, Oviedo O, Zoltan T (2013) Effect of calcination temperature on structural properties and photocatalytic activity of ceria nanoparticles synthesized employing chitosan as template. J Nanomater. https://doi.org/10.1155/2013/265797

Singh J, Sharma A (2012) Application of response surface methodology to the modeling of cellulase purification by solvent extraction.

Adv Biosci Biotechnol 3:408–416. https://doi.org/10.4236/abb.2012.34058

Singh KP, Gupta S, Singh AK, Sinha S (2011) Optimizing adsorption of crystal violet dye from water by magnetic nanocomposite using response surface modeling approach. J Hazard Mater 186:1462–1473. https://doi.org/10.1016/j.jhazmat.2010.12.032

Srikanth DV, Sridhar DC, Chennupati D, Rao MS (2016) Application of RSM for optimal response of process parameters on machining of CFRP composites by using AJM. Int Conf Electr Electron Optim Tech ICEEOT 1677–1681. https://doi.org/10.1109/ICEEOT.2016.7754970

Teja AS, Koh PY (2009) Synthesis, properties, and applications of magnetic iron oxide nanoparticles. Prog Cryst Growth Charact Mater 55:22–45. https://doi.org/10.1016/j.pcrysgrow.2008.08.003

Thai TMN, Kim SR, Kim HJ (2014) Synthesis of Fe$_2$O$_3$ polymorph thin films via a pulsed laser deposition technique. New Phys Sae Mulli 64:252–255. https://doi.org/10.3938/NPSM.64.252

Umar A, Akhtar MS, Dar GN, Baskoutas S (2013) Low-temperature synthesis of α-Fe2O3 hexagonal nanoparticles for environmental remediation and smart sensor applications. Talanta 116:1060–1066. https://doi.org/10.1016/j.talanta.2013.08.026

Wan Isahak WNR, Che Ramli ZA, Mohamed Hisham MW, Yarmo MA (2015) The formation of a series of carbonates from carbon dioxide: capturing and utilisation. Renew Sustain Energy Rev 47:93–106. https://doi.org/10.1016/j.rser.2015.03.020

Wang GH, Li WC, Jia KM, Spliethoff B, Schüth F, Lu AH (2009) Shape and size controlled α-Fe$_2$O$_3$ nanoparticles as supports for gold-catalysts: synthesis and influence of support shape and size on catalytic performance. Appl Catal A Gen 364:42–47. https://doi.org/10.1016/j.apcata.2009.05.030

Xie K, Guo M, Huang H, Liu Y (2014) Fabrication of iron oxide nanotube arrays by electrochemical anodization. Corros Sci. https://doi.org/10.1016/j.corsci.2014.07.019

Xu Y, Yang S, Zhang G, Sun Y, Gao D, Sun Y (2011) Uniform hematite α-Fe$_2$O$_3$ nanoparticles: morphology, size-controlled hydrothermal synthesis and formation mechanism. Mater Lett 65:1911–1914. https://doi.org/10.1016/j.matlet.2011.03.085

Xu H, Sun M, Liu S, Li Y, Wang J, Chen Y (2017) Effect of the calcination temperature of cerium-zirconium mixed oxides on the structure and catalytic performance of WO$_3$/CeZrO$_2$ monolithic catalyst for selective catalytic reduction of NOx with NH3. RSC Adv 7:24177–24187. https://doi.org/10.1039/c7ra03054a

Zhang Z, Zheng H (2009) Optimization for decolorization of azo dye acid green 20 by ultrasound and H$_2$O$_2$ using response surface methodology. J Hazard Mater 172:1388–1393. https://doi.org/10.1016/j.jhazmat.2009.07.146

Zhang P, Guo ZP, Liu HK (2010) Submicron-sized cube-like α-Fe$_2$O$_3$ agglomerates as an anode material for Li-ion batteries. Electrochim Acta 55:8521–8526. https://doi.org/10.1016/j.electacta.2010.07.078

Zhang GY, Feng Y, Xu YY, Gao DZ, Sun YQ (2012) Controlled synthesis of mesoporous α-Fe$_2$O$_3$ nanorods and visible light photocatalytic property. Mater Res Bull 47:625–630. https://doi.org/10.1016/j.materresbull.2011.12.032

Zhang Y, Qu Y, Wang J (2018) Effect of crystal size on the catalytic performance of HZSM-5 zeolite in the methanol to aromatics reaction. Pet Sci Technol 36:898–903. https://doi.org/10.1080/10916466.2018.1451889 https